

Wrapping Thick Membranes with Slipping Folds

Manan Arya*, Nicolas Lee† and Sergio Pellegrino‡

California Institute of Technology, Pasadena, CA 91125

A novel method of packaging finite-thickness membranes tightly and with high packaging efficiency is presented. This method allows the membrane to be packaged without extension and without plastic creasing. As such, initially flat membranes can be deployed to a flat state. Membrane thickness is accommodated by removing material along fold lines and exploiting the slipping deformation mechanism thus created.

Also presented are methods for prestressing and deploying membranes packaged according to this technique. Initial tests demonstrate packaging efficiencies of 73% without plastic deformation. Experimental deployment tests of a meter-scale model showed controlled deployment with unfolding forces of less than 0.6 N.

Nomenclature

A	Area	$\alpha(s)$	Involute angle
a	Diagonal length along x -axis	γ	Packaged radius normalized by h
\bar{a}	Partially deployed length along x -axis	η	Packaging efficiency
b	Diagonal length along y -axis	θ	Involute clock angle
\bar{b}	Partially deployed length along y -axis	$\kappa(s)$	Signed curvature
E	Young's modulus	λ	Length normalized by h
F	Tensioning or deployment force	ξ	Slip along fold line
f	Pitch of involute curve	ρ	Fold angle
$f(x)$	Edge profile	σ_y	Yield stress
H_p	Packaged height	ϕ	Thickness multiplier
h	Thickness	ψ	R_{min} normalized by h
i	Strip index		
L	Side length		
n	Number of strips		
$\mathbf{n}(s)$	Normal to base curve		
P	Prestress per unit length		
$\mathbf{p}(s)$	Generator curve		
$q(i)$	Strip offset from base curve		
R	Radius of generator curve		
R_{min}	Elastic radius of curvature		
R_p	Packaged radius		
$\mathbf{r}(s)$	Base curve		
s	Arclength of the base curve		

I. Introduction

MEMBRANES are widely used for space applications requiring large area surfaces with low areal density. Solar arrays, solar sails, drag sails, reflectors, transmissive optics, and thermal shields are all examples of

*Graduate Student, Graduate Aerospace Laboratories. MC 205-45. AIAA Student Member.

†W. M. Keck Institute for Space Studies Postdoctoral Scholar in Aerospace. MC 301-46. AIAA Member.

‡Joyce and Kent Kresa Professor of Aeronautics and Professor of Civil Engineering, Graduate Aerospace Laboratories. MC 301-46. AIAA Fellow.

large-area structures that may be constructed using membranes. Many applications require these structures to be tightly packaged for launch and deployed to their operational state after launch into space, which raises several fundamental challenges.

Prime among them are efficient packaging, i.e. packaging with only minimal volume gaps in the folded package, packaging without exceeding the yield stress of the membrane, and ability to deploy the membrane to a flat state with minimal edge forces. This paper presents a packaging scheme that addresses all of these challenges in a novel way.

The current practice in membrane packaging is to use localized bending deformation, known as *creasing*, as the basic mechanism for compaction. An alternative approach is proposed, based on the removal of material along the fold lines. This approach provides additional deformation mechanisms and hence enables a new class of packaging solutions.

This paper is organized thus. Section II presents a brief survey of the state of the art on the packaging of membrane structures. A new concept for packaging, deploying, and prestressing is presented in Section III, Section IV, and Section V. Finally, Section VI describes the packaging and deployment tests that were conducted to demonstrate and verify the proposed concept, and Section VII presents and discusses their results.

II. Background

This section reviews existing membrane packaging solutions. These can be divided into two categories: those that compact the membrane along one dimension, and those that compact the membrane along two dimensions.

II.A. 1D Compaction

Three well-known techniques are used for packaging large-area space structures along one dimension: z-folding, wrapping (or rolling), and fan-folding. These techniques provide efficient packaging and easily accommodate for membrane thickness; plastic deformation can be avoided by choosing a suitably large radius of wrapping or folding. However, compaction occurs in one dimension only, and hence these techniques are not applicable when both dimensions of the deployed structure exceed the available packaging envelope.

II.B. 2D Compaction

Miura-ori¹ is a well-known scheme for biaxially packaging a membrane. It modifies the standard map folding technique (i.e. double z-folding) by skewing one set of parallel fold lines. Both map folding and Miura-ori have been used for packaging space structures;^{2,3} however, neither map folding nor Miura-ori accommodate for membrane thickness.

It is also possible to compact membranes along two dimensions by first folding and then wrapping. Both z-folding and wrapping,⁴ and star folding and wrapping⁵ have been used to package membrane space structures. Folding and wrapping requires curved creases to accommodate the thickness of the membrane;^{6,7} however, curved creases do not preserve the flatness of the membrane. In fact, it is impossible for any membrane that has been creased plastically to be pulled completely flat.^{8,9}

Techniques for wrapping a membrane around a polygonal hub using straight creases have been proposed.^{11,12} These techniques generate crease patterns by modeling the wrapped membrane as a collection of straight line creases intersecting at vertices. By placing the vertices set distances apart in the folded state, the crease lengths and angles can be computed. Although these patterns provide, on average, the required accommodation for the thickness of the membrane, the solution is not exactly correct near the fold lines or at the vertices.

It is possible to make these solutions exact by trimming away material. As seen in Figure 1a,¹⁰ an ideal zero-thickness fold pattern, denoted by the red line, can be applied to a finite thickness membrane, denoted by the black outline, by trimming away material close to the fold lines and vertices. However, as the final fold angle decreases, more and more material must be trimmed away; in the limit as the final fold angle goes to zero, all material must be removed. In practice, because it is impossible to decrease the thickness of the membrane to zero, the packaging efficiencies achievable are limited. This technique also requires panels of non-uniform thickness, which may be troublesome for engineering applications.

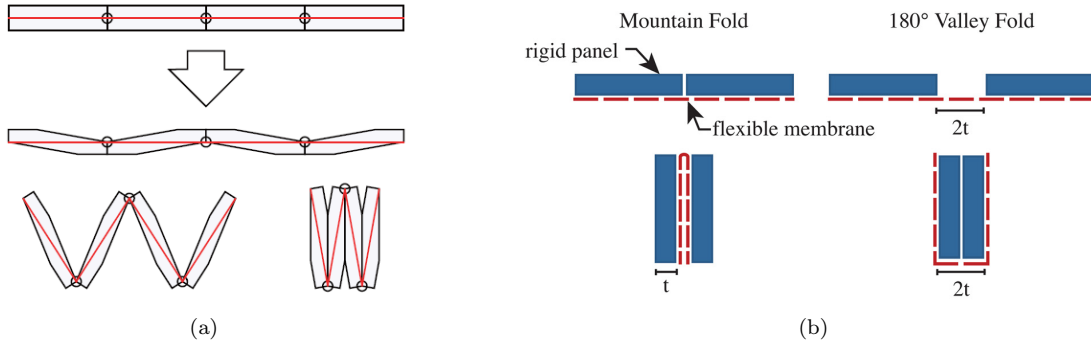


Figure 1: (a) Thickness reduction near the fold lines allows packaging using the ideal zero-thickness crease pattern denoted by the red line.¹⁰ (b) An alternative method is to widen the creases; the width of the crease depends on the final folded angle.¹²

Instead of removing material, it has been proposed to widen and reduce the thickness of the crease regions.^{12,13} However, this results in the presence of large voids in the packaged membrane. Crease widths of 10 to 14 times the panel thickness were required in previous studies to enable packaging.¹²

Hoberman's modifications¹⁴ of Miura-ori allow for the folding of thick membranes. However, these modified patterns also result in gaps between membrane faces in the folded state, and the size of these gaps grows with the size of the membrane, leading to loss of packaging efficiency.

Trautz and Künstler¹⁵ propose a degree-4 vertex in a thick membrane enabled by sliding hinges along the crease lines. Their scheme requires the creases to slide by an infinite amount as the crease angle tends to zero. For this reason, their method does not result in tight and efficient packaging.

In concluding this brief review, it should be noted that there have been several proposals for packaging techniques for thin shell structures that use either radial or spiral cuts.^{16,17,18} Cuts introduce additional deformation mechanisms that enable efficient packaging schemes that accommodate thickness, which is a theme central to the present paper.

III. Packaging Concept

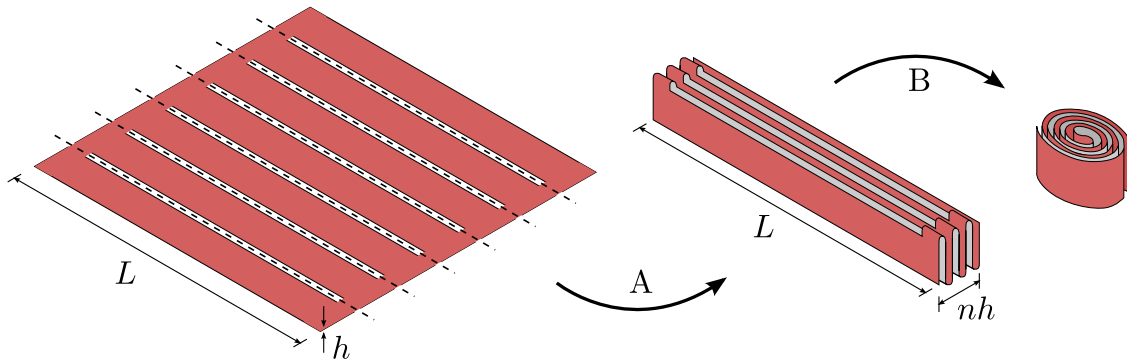


Figure 2: Packaging concept consisting of two steps: (A) z-folding and (B) symmetric wrapping. First, the square membrane is z-folded using $n - 1$ slipping folds. Then, the resulting stack of n strips is wrapped in a rotationally symmetric fashion. For clarity, only a single strip is shown in the wrapped configuration.

To illustrate the basic concept, consider the problem of packaging a square membrane of side length L and thickness h as shown in Figure 2. The membrane is divided into n strips by $n - 1$ slipping folds. A *slipping fold* allows for rotation about the fold line as well as slip along the fold line. In Figure 2 the slipping folds are realized by cutting a series of parallel slits in the membrane, but the continuity of the membrane is maintained at either end of each fold line.

The packaging concept has two compaction steps, each compacting the membrane along a single dimension. For the first step, the membrane is z-folded using parallel slipping folds, which produces a stack of n

strips. For the second step, this stack of strips is wrapped in a rotationally symmetric fashion.

The slipping folds are needed to accommodate the incompatibility created by wrapping the thick membrane strips around different radii. The symmetric wrapping scheme ensures that the ends of the strips can remain connected. The following two subsections will explain in detail the two enabling concepts of slipping folds and symmetric wrapping.

III.A. Slipping Folds

The proposed packaging concept relies on material removal along fold lines to create *slipping folds*. The membrane can be folded and unfolded at such slipping folds without straining the material. In some sense, a slipping fold is an extreme case of a score; whereas a score weakens the membrane to localize bending strains, a slipping fold removes material entirely.

The two degrees of freedom of a slipping fold are shown in Figure 3. In addition to the fold angle, ρ , slipping folds have a slip degree of freedom, ξ , which is the linear displacement of the material on one side of the fold with respect to the material on the other side, in the direction of the fold line. An ideal slipping fold has zero stiffness associated with both these degrees of freedom.

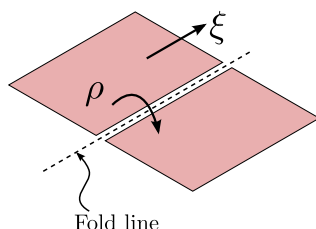


Figure 3: Slipping folds have two degrees of freedom: fold angle ρ and slip ξ .

Because material removal along the fold lines leads to a reduction in the continuity and hence in the stiffness of a structure, several realizations of slipping folds have been considered that are not simple cuts. These realizations include connections that allow for the transmission of tension forces and the limited transmission of shearing forces across fold lines. Figure 4 illustrates two possible methods for forming these connections.

Hinged fold A cylindrical rod is located at the fold line. This rod is attached to the material on one side of the fold using tabs. The material on the other side is attached to the rod using a loop. This loop can rotate about the rod and slip along the rod. Maximum slip is reached when the loop contacts a tab. A hinged fold transmits tension across the fold line. In the maximum slip state, a shearing force may also be transmitted.

Ligament fold To create a ligament fold, one or more thin strips of material are left uncut at the fold line. The length of the ligament is chosen to allow for the required deformation along the fold line. Like the hinged fold, a ligament fold has state of maximum slip beyond which the ligament will deform plastically. A ligament fold allows for the transmission of tension and shear across the fold line.

The slip degree of freedom is crucial; it enables the second compaction step of wrapping. Wrapping the z-folded stack of n strips leads to the outer strips going around larger radii than the inner strips because each strip has thickness $h > 0$. Thus, for the same arclength, outer strips traverse smaller wrapping angles than inner layers. If the strips cannot slip against each other, wrapping the stack of strips will result in straining of the membrane.

In addition to areas where the membrane strips can slip against each other, it is also advantageous to constrain the slip to be zero at certain locations, which allows the strips to be connected at the ends. This condition can be achieved by using a rotationally symmetric wrapping.

III.B. Symmetric Wrapping

Symmetric wrappings are a class of wrappings that result in a configuration that has two-fold symmetry. Using these wrappings, it is possible to enforce zero slip, for example, at the two ends of the z-folded stack, which enables the edges of the membrane to remain uncut and able to transmit tension. The ability of

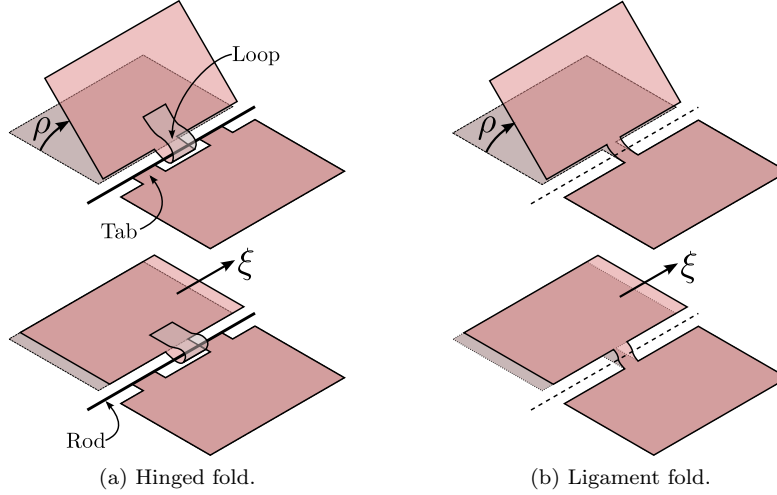


Figure 4: Two examples of slipping folds with connections across the fold lines that still allow for the rotation and slip degrees of freedom.

the edges to transmit tension will be useful when a concept for prestressing the membrane are discussed in Section IV.

The membrane strips in the wrapped stack are modeled as a set of curves offset from a *base curve*. (If the number of strips n is odd, the base curve corresponds to the middle strip.)

The base curve $\mathbf{r}(s) : [-L/2, L/2] \rightarrow \mathbb{R}^2$ is parametrized by its arclength s . As shown in Figure 5, the i^{th} strip is offset from the base curve by $q(i)\mathbf{n}(s)$, where $\mathbf{n}(s)$ is the normal to the base curve and $q(i)$ is a separation distance. (If n is odd, $q(i) = ih$.) Thus the i^{th} strip follows the offset curve $\mathbf{r}(i; s) = \mathbf{r}(s) + q(i)\mathbf{n}(s)$.

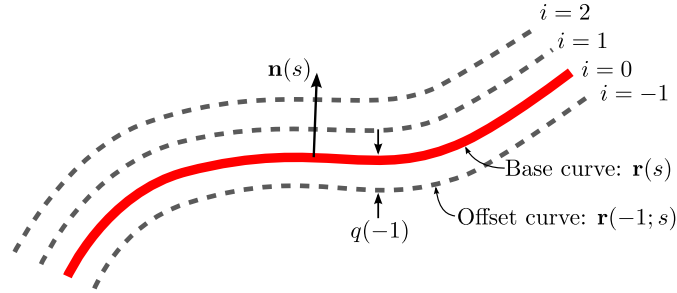


Figure 5: Offset curves separated by a normal distance $q(i)$.

For the ends of the strips to be connected, the length of the i^{th} strip L_i must equal the length of the base curve L for all i . This is possible when the integral of the signed curvature $\kappa(s)$ of the base curve is zero. To see this, consider the formula for the length L_i of the i^{th} strip:

$$L_i = \int_{-L/2}^{L/2} \|\mathbf{r}'(i; s)\| ds \quad (1)$$

$$\|\mathbf{r}'(i; s)\| = \|\mathbf{r}'(s) + q(i)\mathbf{n}'(s)\| \quad (2)$$

Now the derivative of the normal vector $\mathbf{n}'(s)$ is parallel to the tangent vector $\mathbf{r}'(s)$ and has length $|\kappa(s)|$:¹⁹

$$\mathbf{n}'(s) = -\kappa(s)\mathbf{r}'(s) \quad (3)$$

Substituting this into the expression for $\|\mathbf{r}'(i; s)\|$ and noting that $\|\mathbf{r}'(s)\| = 1$ gives

$$\|\mathbf{r}'(i; s)\| = 1 - q(i)\kappa(s) \quad (4)$$

$$\Rightarrow L_i = \int_{-L/2}^{L/2} [1 - q(i)\kappa(s)] ds = L - q(i) \int_{-L/2}^{L/2} \kappa(s) ds \quad (5)$$

Thus, for $L_i = L \forall i$ the following condition must be satisfied:

$$\int_{-L/2}^{L/2} \kappa(s) ds = 0 \quad (6)$$

A simple way to meet this condition is to have $\kappa(s)$ be an odd function of arclength, i.e. $-\kappa(-s) = \kappa(s)$. A base curve that has this may be defined in a piecewise manner, using a *generator curve* $\mathbf{p}(s) : [0, L/2] \rightarrow \mathbb{R}^2$ and a copy of the generator curve rotated by 180° :

$$\mathbf{r}(s) = \begin{cases} -\mathbf{p}(-s) & \text{if } s \in [-L/2, 0) \\ \mathbf{p}(s) & \text{if } s \in [0, L/2] \end{cases} \quad (7)$$

For $\mathbf{r}(s) \in C^2$, $\mathbf{p}(s) \in C^2$, $\mathbf{p}(0) = \mathbf{0}$ and $\mathbf{p}''(0) = \mathbf{0}$ are needed.

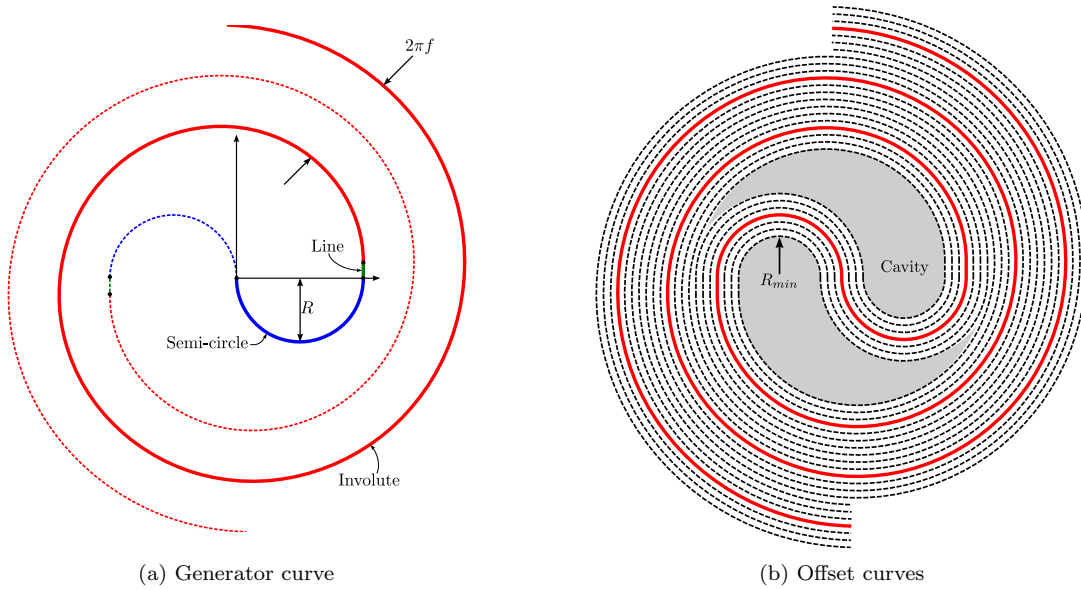


Figure 6: Wrapping curve for efficient packaging. The shaded areas in (b) are the only cavities that result from this curve, and their size depends mainly on the minimum radius of curvature R_{min} .

A generator curve that allows for compact wrapping is shown in Figure 6. It is a piecewise curve consisting of a semi-circle of radius R , a vertical line of length f , and an involute of a circle with pitch $2\pi f$:

$$\mathbf{p}(s) = \begin{cases} R \{1 - \cos(s/R), -\sin(s/R)\} & \text{if } s \in [0, \pi R] \\ R \{2, (s/R) - \pi\} & \text{if } s \in (\pi R, \pi R + f) \\ f \{ \cos(\alpha - \theta) + \alpha \sin(\alpha - \theta), \\ \sin(\alpha - \theta) - \alpha \cos(\alpha - \theta) \} & \text{if } s \in (\pi R + f, L/2) \end{cases} \quad (8)$$

$$\alpha^2 = \frac{2}{f} (s - \pi R - f) + \left(\frac{2R}{f}\right)^2 \quad (9)$$

$$\theta = \frac{2R}{f} - \frac{\pi}{2} \quad (10)$$

Note that this particular generator curve has discontinuous curvature at all points where two pieces meet. Therefore it is not expected that a wrapped membrane will follow this curve exactly; however, it is a simple curve that may be used to estimate the size of the packaged membrane, which will be contained within a cylinder of radius R_p and height H_p .

A strip thickness multiplier $\phi \geq 1$ is included to account for the fact that in the packaged configuration the strips may be separated by some distance $\phi h \geq h$. The pitch of the involute $2\pi f = 2n\phi h$ accounts for

the thickness of the z-folded stack of strips. The radius of the semi-circle $R = R_{min} + \phi hn/2$ is such that the curvature limit $1/R_{min}$, dictated by the material modulus E and yield stress σ_y , is not exceeded:

$$\frac{1}{R_{min}} = \frac{2\sigma_y}{Eh} \quad (11)$$

III.C. Packaging Efficiency

The packaged radius is $R_p = \max \|\mathbf{r}(i; s)\|$ and the packaged height is $H_p = L/n$. Using these, the packaging efficiency η , which is the ratio of the packaged volume to the material volume of the membrane, can be estimated.

$$\eta = \frac{L^2 h}{\pi R_p^2 H_p} \quad (12)$$

The packaging efficiency is a function for four non-dimensional parameters: n , $\psi \equiv R_{min}/h$, $\lambda \equiv L/h$, and ϕ . It has the following expression:

$$\eta = \frac{n\lambda}{\pi\gamma^2} \quad (13)$$

$$\gamma^2 \equiv \left(\frac{R_p}{h}\right)^2 = \phi^2 \left[\left(\frac{n}{\pi}\right)^2 + \left(\frac{n\alpha_{max}}{\pi}\right)^2 + \left(\frac{n-1}{2}\right)^2 + \frac{n(n-1)}{\pi}\alpha_{max} \right] \quad (14)$$

$$\alpha_{max}^2 = \frac{\pi\lambda}{n\phi} + \frac{2\pi^2\psi}{n\phi} - 2 + \left(\frac{2\pi\psi}{n\phi}\right)^2 \quad (15)$$

Figure 7 shows the variation of the packaging efficiency with λ , ψ , and ϕ . The effect of n on the packaging efficiency is minimal, since as n increases, the packaged height decreases, but the packaged radius increases, and thus the packaged volume varies minimally.

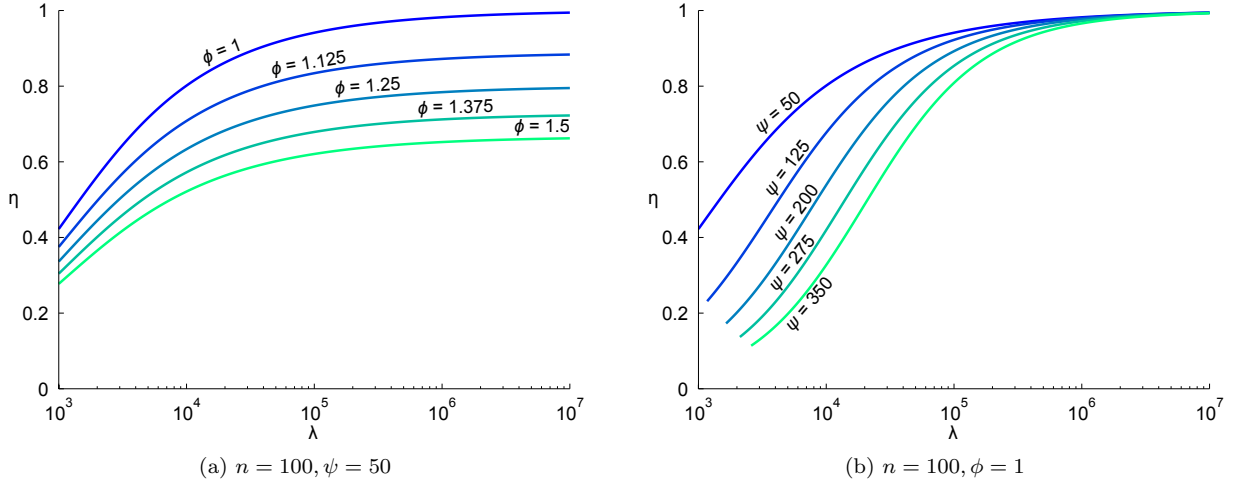


Figure 7: Packaging efficiency η as a function of the dimensionless deployed length $\lambda = L/h$, the dimensionless minimum bend radius $\psi = R_{min}/h$, and the strip thickness multiplier ϕ . For (a), n and ψ are held constant, and for (b), n and ϕ are held constant.

Figure 7a shows that the strip thickness multiplier ϕ has the greatest effect on the packaging efficiency for large λ . In fact, in the limit of $\lambda \rightarrow \infty$, $\eta \rightarrow 1/\phi$. This means that for very large or very thin membranes, the global packaging efficiency depends only on the local, per-strip packaging efficiency. Figure 7b shows that the minimum bend radius of the material $R_{min} = h\psi$ has the greatest effect for small λ . As λ increases, the size of the two cavities (which is determined by R_{min}) shown in Figure 6 shrinks in relation to the membrane volume and the effect of ψ decreases.

IV. Prestressing Concept

A membrane with slipping folds is anisotropic; the stiffness parallel to the slipping folds is much higher than the stiffness perpendicular to them. This anisotropy must be taken into account when prestressing the membrane. This section presents one particular solution to the problem of prestressing membranes of this type.

Consider a membrane as shown in Figure 8a with slipping folds parallel to the y -axis, length a along the x -axis and length b along the y -axis. When prestressed, it is desired that each strip has equal tension in the y -direction, i.e. parallel to the slipping folds, and no tension in the x -direction, i.e. perpendicular to the slipping folds.

Consider applying global tensioning forces F_x at $[\pm a/2, 0]$ and F_y at $[0, \pm b/2]$ (using suitable external compression members e.g. booms or masts); the membrane edges can be shaped such as to distribute these tensioning forces to uniaxial tensile loading P , which is a force per unit length. Since the symmetric wrapping ensures that the edges of the membrane remain continuous and uncut, they can transmit tension. It is easy to show that for P uniform, the edge profile $f(x) : [0, a/2] \rightarrow \mathbb{R}$ must be parabolic:

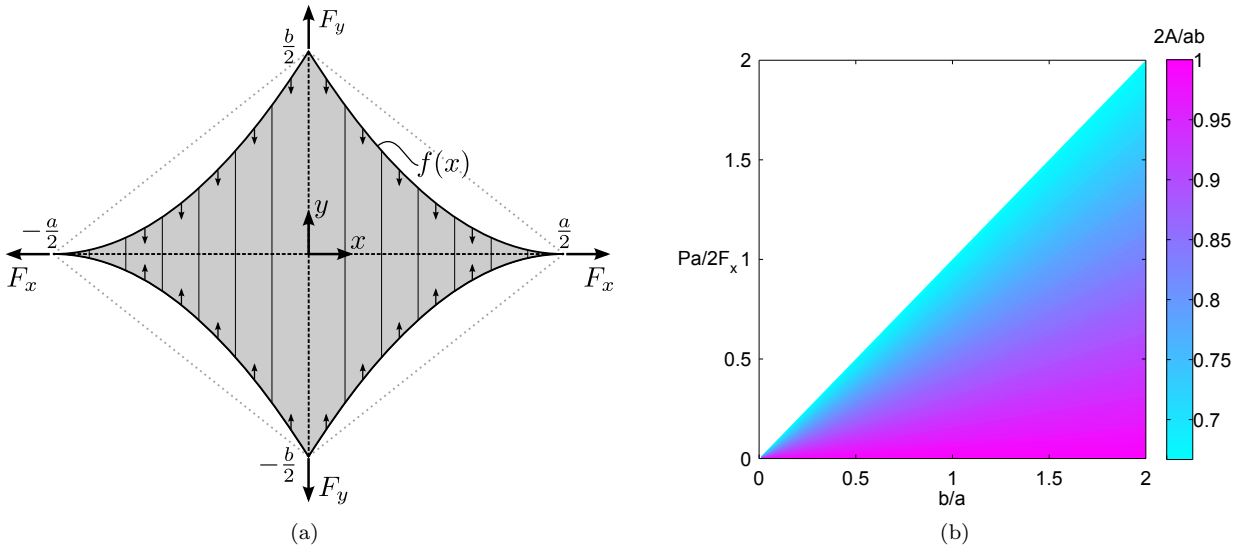


Figure 8: (a) Membrane with parabolic edges tensioned uniformly and uniaxially by four radial forces. (b) Membrane area A normalized by the rhombus area $ab/2$ as function of the aspect ratio b/a and the normalized loading $Pa/2F_x$. The white triangle is inaccessible due to $f'(a/2) \leq 0$.

$$f(x) = \left(\frac{P}{F_x}\right) x^2 - \left(\frac{Pa}{2F_x} + \frac{b}{a}\right) x + \frac{b}{2} \quad (16)$$

The edges of the membrane can be constructed by taking $f(x)$ and mirroring it about the x and y axes. To ensure $f(x) \geq 0$, it is insisted that $f'(a/2) \leq 0$, and hence

$$\frac{Pa}{2F_x} - \frac{b}{a} \leq 0 \quad (17)$$

Two non-dimensional parameters, the loading parameter $Pa/2F_x$ and the aspect ratio b/a , determine key aspects of this structure. The membrane area A normalized by the rhombus area $ab/2$ is a function of these parameters, as is the ratio of the global tensioning forces F_y/F_x :

$$\frac{2A}{ab} = 1 - \frac{1}{3} \frac{a}{b} \frac{Pa}{2F_x} \quad (18)$$

$$\frac{F_y}{F_x} = \frac{Pa}{2F_x} + \frac{b}{a} \quad (19)$$

Figure 8b plots the dimensionless area as a function of these two parameters.

V. Deployment Concept

This section discusses a particular concept for deploying a slip-wrapped membrane with parabolic edges. The deployment concept, shown in Figure 9, consists of an unwrapping stage followed by an unfolding stage.

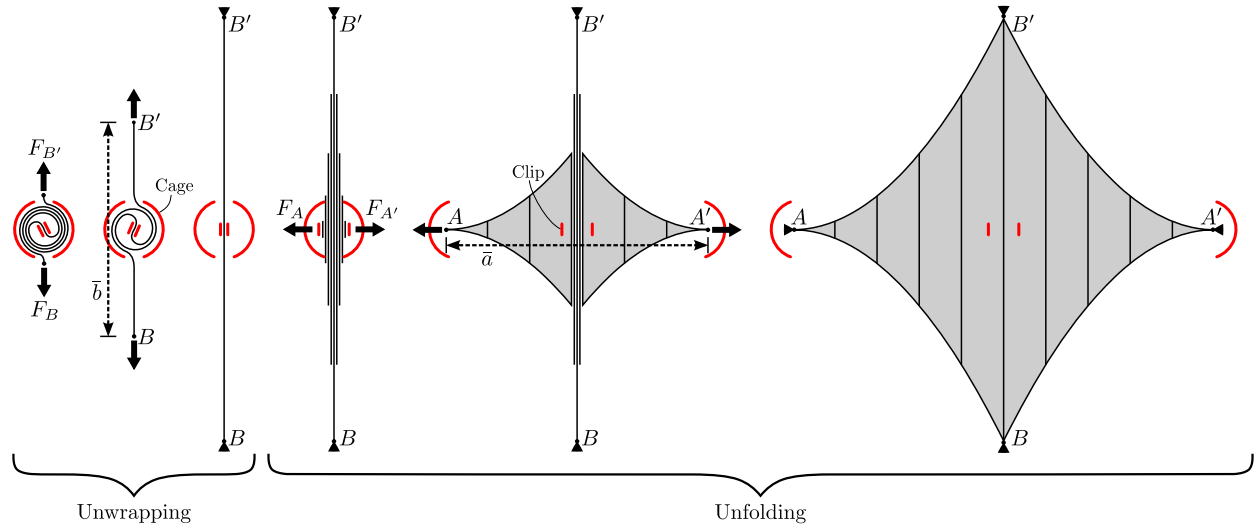


Figure 9: The two stages of deploying a slip-wrapped membrane with parabolic edges. For clarity, just one strip is shown during the unwrapping stage.

In the unwrapping stage, the two ends B and B' of the wrapped stack are pulled in opposite directions by applying forces F_B and $F_{B'}$. The separation \bar{b} between B and B' increases until $\bar{b} = b$.

In the unfolding stage, the stack of strips is unfolded by applying forces F_A and $F_{A'}$ at points A and A' . The separation between these points \bar{a} grows to a at the end of deployment.

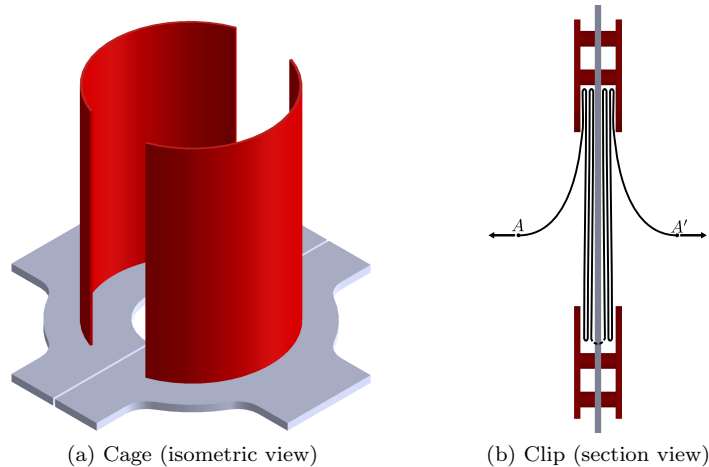


Figure 10: Deployment restraints.

A “cage”, shown in Figure 10a, is used to manage the unwrapping process. It is a cylindrical tube with two slots. The endpoints B and B' of the folded membrane stack are pulled out through these slots. During the unfolding stage, the two halves of the cage must separate and move apart, see Figure 9.

A “clip”, shown in Figure 10b, holds the folded stack of the strips together at midpoint. It manages the unfolding stage; it ensures that when the endpoints A and A' of the folded stack are pulled outwards, the strips deploy one at a time. The wrapped membrane rotates with respect to the cage during the unwrapping stage, and hence the clip has to rotate as well.

An experimental implementation of this concept is presented in the following section.

VI. Test Apparatus and Procedures

VI.A. Packaging Tests

To wrap a membrane according to the technique described in Section III, a “wrapping plug” can be used to guide the folded membrane stack along the designed curve and prevent the membrane from exceeding the maximum curvature limit as provided by Equation (11). Figure 11a shows a conceptual plug; it consists of two halves shaped like the cavities in the wrapping curve of Figure 6.

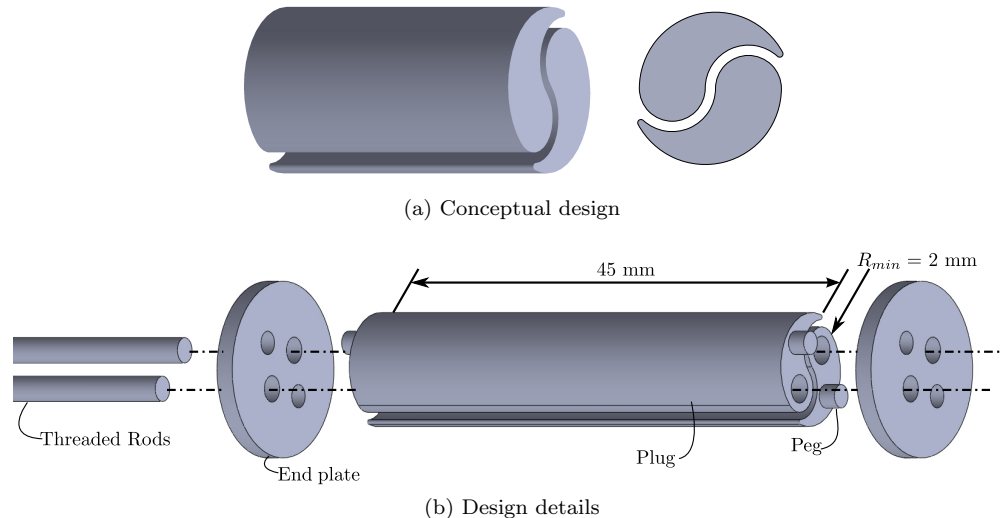


Figure 11: Wrapping plug.

A wrapping plug suitable for polyester films of thickness of up to $50.8\ \mu\text{m}$ was designed. Assuming $E = 3.50\ \text{GPa}$ and $\sigma_y = 100\ \text{MPa}$ for polyester films, Equation (11) gives R_{min} of $0.89\ \text{mm}$. However, fabrication constraints imposed an upper bound on R_{min} of $2\ \text{mm}$, and therefore there was a margin of safety of 2.25 against plastic deformation in the membrane. A detailed design of the wrapping plug with $R_{min} = 2\ \text{mm}$ and a length of $45\ \text{mm}$ is shown in Figure 11b.

The two halves of the plug were fabricated from UV-curable acrylic plastic using stereolithography. Each half of the plug has a lengthwise hole to accept a threaded rod. Each half also has small pegs at either end that mate with two end plates. These end plates hold the two halves of the plug in alignment. Two threaded rods are passed through the lengthwise holes in the plugs and the end plates, and are held in place by nuts.

Two square models were made from aluminized polyester film and wrapped around this plug. Table 1 lists the relevant parameters of these models. These models had ligament slipping folds made using a computer-controlled laser cutter (Universal Laser Systems[®] ILS9.75). There were 7 ligaments per fold line. The ligaments had widths of $1.5\ \text{mm}$, lengths of $8\ \text{mm}$, and rounded corners.

Model	h (μm)	L (m)	$\log_{10}(\lambda)$	n	ψ
1	25.4	0.5	4.3	13	78.7
2	50.8	0.5	4.0	13	39.4

Table 1: Packaging models

To package the membrane, it was first folded into a stack of strips. The strips were then pre-slipped with respect to each other at the middle of the stack by $1.1\ \text{mm}$ and $1.7\ \text{mm}$ respectively for models 1 and 2. This pre-slip was induced before the membrane stack was inserted into the plug. When packaging without a plug, this step of pre-slipping is not required, since the strips are free to slip during packaging. However, the plug tightly clamps the strips against each other and prevents slip from developing during packaging. Therefore, it was necessary to pre-slip the strips.

The strips were then manually wrapped tightly against the plug. A loop of string was used to hold the membrane wrapped while a digital caliper was used to measure the packaged diameter at the middle of the wrap. Figure 12 shows model 2 wrapped around the plug.



Figure 12: Model 2 wrapped around the plug. The packaged diameter was 23.92 mm.

VI.B. Prestressing Test

To demonstrate the feasibility of the prestressing concept, an aluminized polyester film model with $b/a = Pa/2F_x = 1$, $a = 0.8$ m, $h = 50.8 \mu\text{m}$ was made. The parabolic edge and the ligament slipping folds were made using the laser cutter. Since $b/a = Pa/2F_x = 1$, $F_y/F_x = 2$.

Figure 13 shows the model hanging on a metal-backed chalkboard using magnets. The tensioning forces were applied by hanging weights: F_y was applied by hanging a 50 g weight and pinning the top corner of the membrane and F_x was applied through a pulley by hanging a 25 g weight and pinning the right corner of the membrane.

Inspection of the model showed that each strip was in a state of tension, and that the model was able to hang flat, though there was some residual transverse curvature of the strips from the film having been stored on a roll.

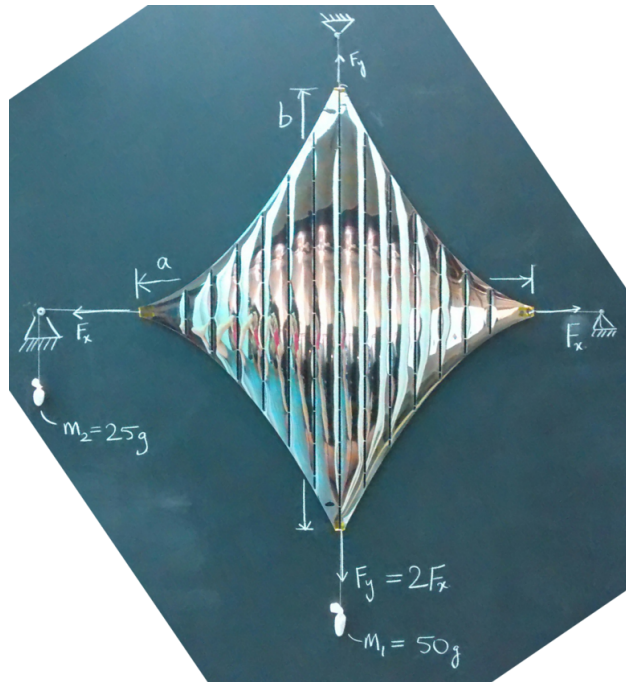


Figure 13: Hanging model test of prestressing concept.

VI.C. Deployment Test

To test the deployment concept presented in Section V, a membrane model with parabolic edges and ligament slipping folds was fabricated. The model had $b/a = Pa/2F_x = 1$, $a = 1$ m, $h = 25.4$ μm , and was made from aluminized polyester film. Because the laser cutter allowed a maximum part size of 0.91 m \times 0.61 m, the model was fabricated in three separate pieces, which were joined together using polyimide tape.

The deployment rig shown in Figure 14 was used to test the deployment concept. It consisted of four independent linear actuators to provide the deployment forces $F_B, F_{B'}, F_A, F_{A'}$, four force sensors to record the deployment forces, and a suspension system to partially offload the mass of the membrane.

Each linear actuator consisted of a lead screw coupled to a stepper motor that drives a carriage back and forth along a rail. Each stepper motor is driven by a separate microstepping driver. A microcontroller synchronized the four motors, as well as providing logic, displacement data logging, and an interface to a PC.

Each carriage had a sensitive six-axis force sensor (ATI Industrial Automation Nano17) that measures deployment force with a resolution of 3.1 μN .

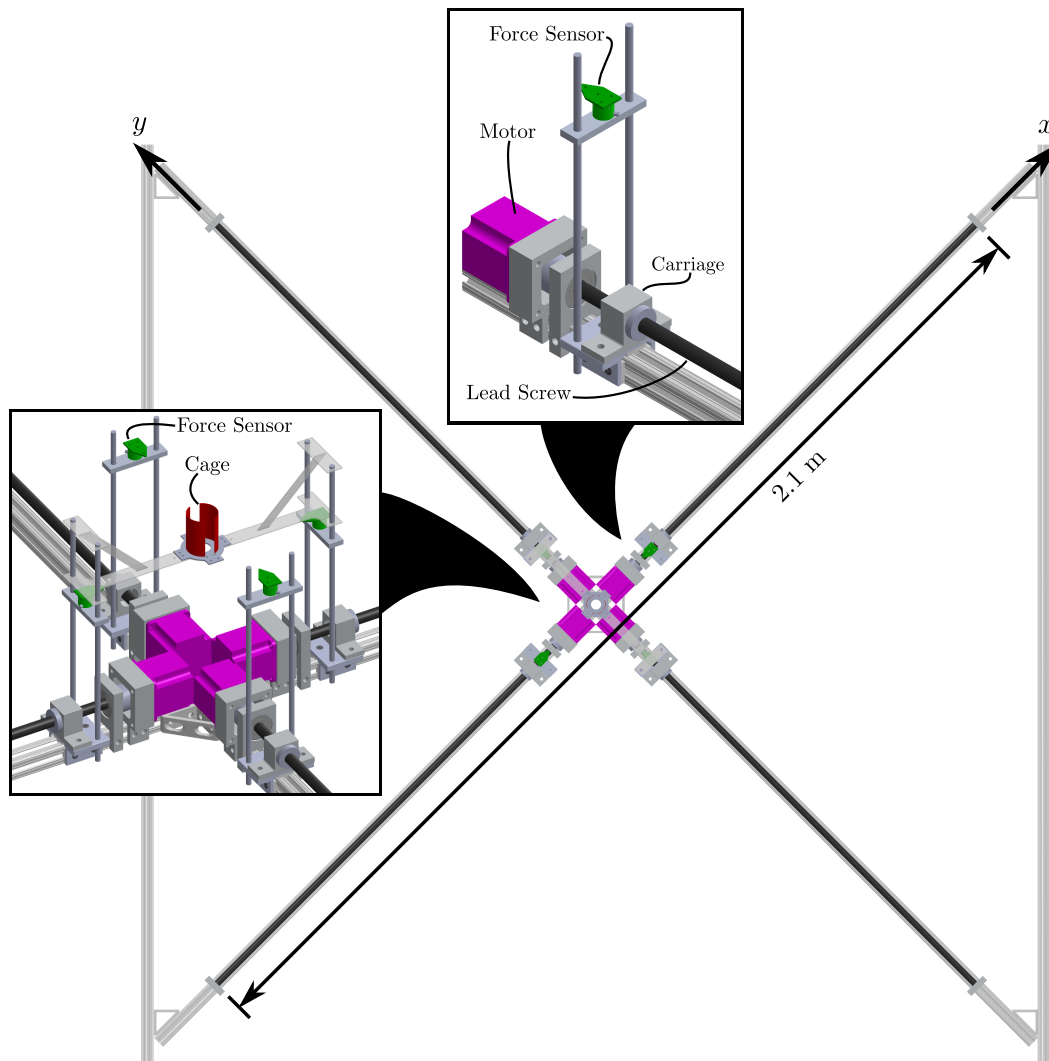


Figure 14: Two-axis deployment rig.

Figure 15 shows the cage and the clip as fabricated. The cage was made of two laser-cut acrylic base plates, 125 μm -thick polyimide rectangular plates elastically bent into half-pipes, and threaded rods to attach the half-pipes to the base plates. The cage was constructed in two halves, which need to separate for the unfolding stage of the deployment. The inside faces of the half-pipes were coated with a dry lubricant to

reduce friction between the cage and membrane during unwrapping.

A clip prototype was made using two paintbrush heads (7 mm \times 4 mm cross section, 11 mm length) connected by a steel rod. The paintbrush bristles were pushed into the middle of the wrapped membrane stack. The membrane strips were spaced apart at this clip insertion point. This separation between the membrane strips ensured that they deployed one by one.

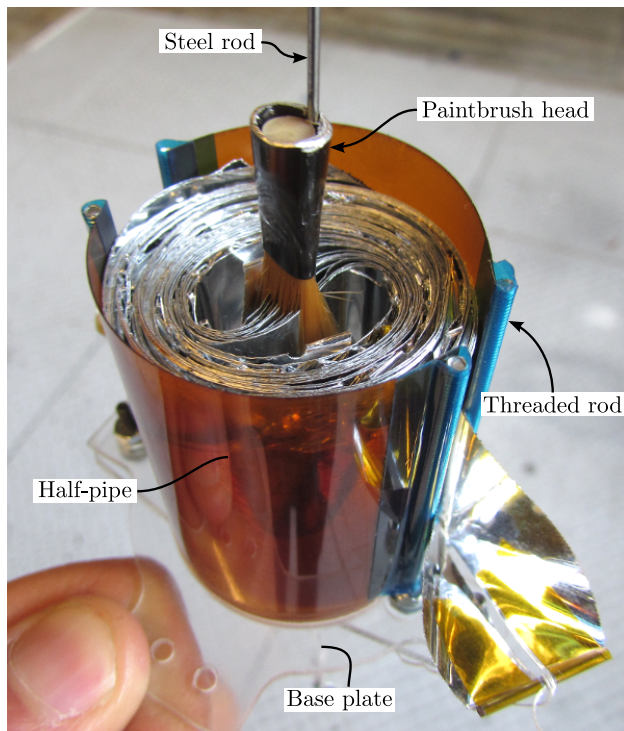


Figure 15: The cage and the clip, as fabricated. The membrane model has been wrapped and inserted into the cage with the clip. The cage half-pipes have a diameter of 37 mm and a height of 49 mm.

To simulate deployment in a 0 g environment, the clip was suspended about 0.25 m above the base of the two-axis deployment rig. Since the clip holds the middle of the membrane during most of the deployment, suspending the clip helped offload some of the weight of the membrane. A 400 g weight was suspended from the bottom of the clip to stabilize its orientation. The membrane weight was also partially offloaded at the attachment to the force sensors. The membrane was deployed in a horizontal plane. However, this setup is only an approximate gravity offload scheme, and it is expected that the measured deployment forces include a component of the membrane weight.

VII. Test Results

VII.A. Packaging Test Results

The two models listed in Table 1 were packaged according to the procedure described in Section VI.A. Their diameters at the middle of the wrapped stack, i.e. away from the ligaments and close to the restraining string, were measured and used to calculate their packaging efficiencies, which are plotted in Figure 16.

Also plotted are lines of varying λ with the same n and ψ values as the models, with ϕ such that these lines pass through the experimental points. These lines represent packaging efficiencies achievable using similar manufacturing and packaging techniques, but scaled to different λ .

VII.B. Deployment Test Results

The membrane model described in Section VI.C was deployed using the two-axis rig. The in-plane radial deployment forces $F_B, F_{B'}, F_A, F_{A'}$ were measured, and are plotted in Figure 17 with respect to the unwrapping deployment fraction \bar{b}/b and the unfolding deployment fraction \bar{a}/a . (The in-plane transverse deployment

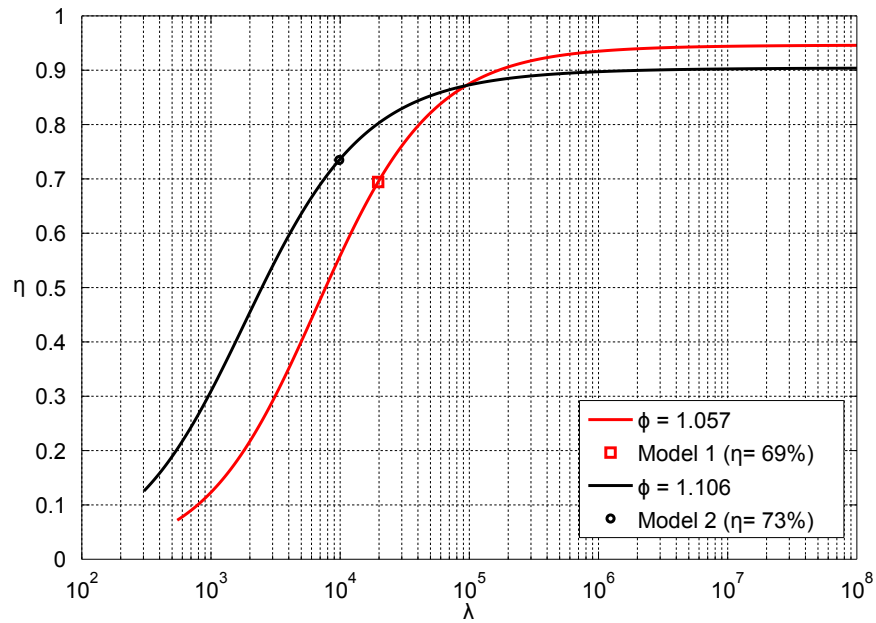


Figure 16: Packaging test results. Packaging efficiency η is plotted with respect to dimensionless deployed length $\lambda = L/h$ for the two packaging models. Also shown are the two packaging efficiency curves with the same values for n and ψ as the packaging models, with the strip thickness multiplier ϕ adjusted such that these curves pass through the experimental points.

forces were about 20 times smaller than the radial forces, and are not shown. The out-of-plane forces are primarily due to the weight of the membrane and are not shown.) The radial component of the deployment forces never exceeded 0.6 N. The deployment was displacement controlled at a rate of about 11.9 mm s^{-1} .

During the unwrapping stage, the deployment forces were largely caused by friction between the wrapped membrane rotating inside the cage and rubbing against the walls of the cage. Note that during the initial stages of unwrapping, $F_{B'} \gg F_B$. This is because pulling on one end of the wrapped stack causes the other end to deploy; in a displacement-controlled deployment any lag between the two ends of the wrapped stack is persistent.

During the unfolding stage, the deployment forces F_A and $F_{A'}$ show a snapping behavior as each strip is deployed from the clip. The separation of these snaps indicates the separate (as opposed to simultaneous) unfolding of each strip. Indeed, that is what was observed: each strip was deployed separately and in sequence.

Figure 18 shows views from an overhead camera at the beginning of deployment, at the end of the unwrapping stage, during the unfolding stage, and at the end of the deployment.

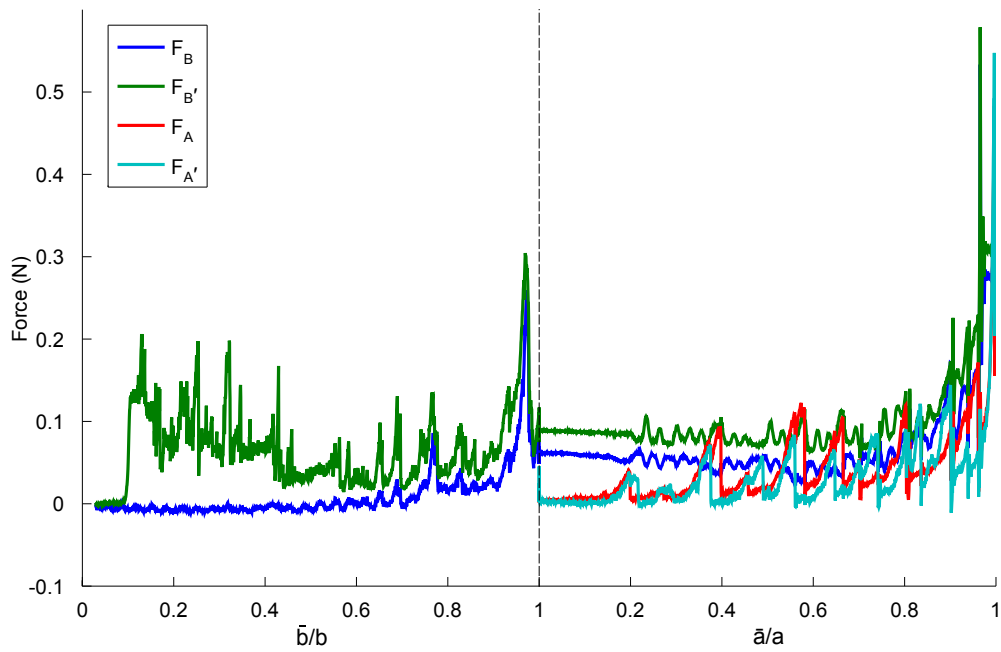
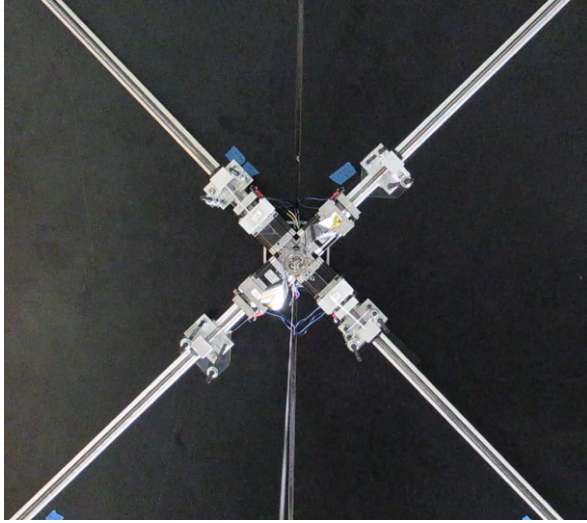


Figure 17: Deployment force profiles. \bar{b}/b is the unwrapping deployment fraction and \bar{a}/a is the unfolding deployment fraction. During the first stage of unwrapping, the unfolding deployment fraction \bar{a}/a is fixed at 0, and during the second stage of unfolding, the unwrapping deployment fraction \bar{b}/b is fixed at 1.



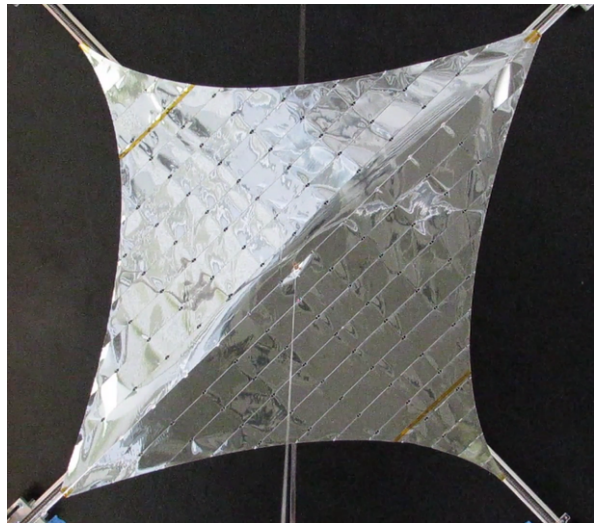
(a) Packaged



(b) Unwrapped



(c) Unfolding



(d) Deployed

Figure 18: Deployment test for a membrane with $a = b = 1$ m, $h = 25$ μ m viewed from an overhead camera.

VIII. Conclusion

A scheme for packaging thick membranes is presented that compacts the membrane along two dimensions by first folding and then wrapping the membrane. This scheme allows the membrane to be packaged tightly, with very few voids, and without plastic creases. Slipping folds are used to accommodate material thickness.

These slipping folds rely on material removal; however, realizations of slipping folds are described that allow for the transmission of tension forces across the fold lines. A two-fold symmetric wrapping scheme is described that allows for the preservation of continuity at the edges of the membrane.

A kinematic model for the wrapped membrane is used to estimate packaging efficiencies, which approaches 100% for tightly wrapped membranes with large length-to-thickness ratios. Packaging tests on 0.5 m-scale models achieved packaging efficiencies of 69% and 73%.

Also presented is a strategy for prestressing a membrane packaged using slipping folds. This strategy uses the continuous edges of the membrane to distribute radial prestress forces into uniform tension parallel to the fold lines. A 0.8 m-scale prototype was used to demonstrate the feasibility of this prestressing strategy.

A two-stage method for deploying a slip-wrapped membrane is proposed. Initial tests conducted on 1 m-scale models showed successful and controlled deployment with low unfolding forces.

Acknowledgments

Support from the Northrop Grumman Corporation is gratefully acknowledged.

N. Lee was supported through this work by a postdoctoral fellowship from the W. M. Keck Institute for Space Studies.

References

- ¹Miura, K., "Method of packaging and deployment of large membranes in space," *Proceedings of the 31st Congress of the International Astronautical Federation IAF-80-A 31 Tokyo*, pp. 1–10, 1980.
- ²Miura, K. and Natori, M. "2-D array experiment on board a space flyer unit," *Space Solar Power Review*, vol. 5, pp. 345–356, 1985.
- ³Biddy, C. and Svitek, T., "LightSail-1 Solar Sail Design and Qualification," *41st Aerospace Mechanisms Symposium*, 2012, pp. 451–463.
- ⁴Montgomery, E. E. I. and Adams, C. L., "NanoSail-D," *CubeSat Developer's Workshop*, 2008.
- ⁵Furuya, H., Mori, O., Okuizumi, N., Shirasawa, Y., Natori, M. C., Miyazaki, Y., and Matunaga, S., "Manufacturing and Folding of Solar Sail IKAROS," *52nd AIAA/ASME/ASCE/AHS/ASC Structures, Structural Dynamics, and Materials Conference*, Apr. 2011.
- ⁶Lee, N. and Close, S., "Curved pleat folding for smooth wrapping," *Proceedings of the Royal Society A: Mathematical, Physical and Engineering Sciences*, vol. 469, issue 2155, 2013.
- ⁷Satou, Y. and Furuya, H., "Fold Line Based on Mechanical Properties of Crease in Wrapping Fold Membrane," *54th AIAA/ASME/ASCE/AHS/ASC Structures, Structural Dynamics, and Materials Conference*, Apr. 2013.
- ⁸Murphey, T. W., *A nonlinear elastic constitutive model for wrinkled thin films*, Ph.D. thesis, 2000.
- ⁹Papa, A. and Pellegrino, S., "Systematically Creased Thin-Film Membrane Structures", *Journal of Spacecraft and Rockets*, Vol. 45, No. 1, 2008, pp. 10-18.
- ¹⁰Tachi, T., "Rigid-Foldable Thick Origami," *Origami 5*, edited by M. Yim, 2011, pp. 253–263.
- ¹¹Guest, S. D. and Pellegrino, S., "Inextensional wrapping of flat membranes," *First International Seminar on Structural Morphology*, Sept. 1992, pp. 203–215.
- ¹²Zirbel, S. A., Lang, R. J., Thomson, M. W., Sigel, D. A., Walkemeyer, P. E., Trease, B. P., Magleby, S. P., and Howell, L. L., "Accommodating Thickness in Origami-Based Deployable Arrays," *Journal of Mechanical Design*, Vol. 135, Nov. 2013, pp. 111005.
- ¹³Reynolds, W. D. and Murphey, T. W., "Elastic Spiral Folding for Flat Membrane Apertures," *55th AIAA/ASME/ASCE/AHS/ASC Structures, Structural Dynamics, and Materials Conference*, Jan. 2014.
- ¹⁴Hoberman, C., "Reversibly Expandable Structures," United States Patent No. 4,981,732, 1991.
- ¹⁵Trautz, M. and Künstler, A., "Deployable folded plate structures folding patterns based on 4-fold-mechanism using stiff plates," *Proceedings of the International Association for Shell and Spatial Structures Symposium*, pp. 2306–2317, Oct. 2009.
- ¹⁶Greschik, G., "Deployment of Dishes with Surface Discontinuities," *Journal of Spacecraft and Rockets*, Vol. 33, No. 4, 1996.
- ¹⁷Tibbalds, B., Guest, S. D., and Pellegrino, S., "Inextensional Packaging of Thin Shell Slit Reflectors," *Technische Mechanik*, Vol. 24, No. 3-4, 2004, pp. 211–220.
- ¹⁸Reynolds, W. D., Murphey, T. W., and Banik, J. A., "Highly Compact Wrapped-Gore Deployable Reflector," *52nd AIAA/ASME/ASCE/AHS/ASC Structures, Structural Dynamics, and Materials Conference*, Apr. 2011.
- ¹⁹Spivak, M., *A Comprehensive Introduction to Differential Geometry*, Vol. II, 3rd ed., 1999.